Article

Current Biology

Adaptive evolution of CENP-T modulates centromere binding

Graphical abstract

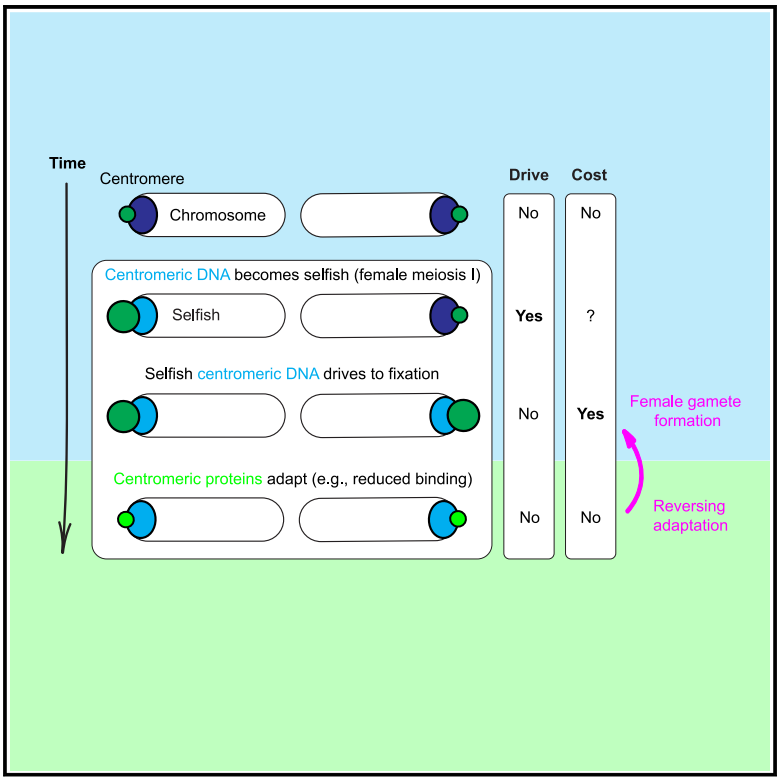

Highlights

- Molecular evolution analysis suggests recurrent adaptation of the rodent CENP-T HFD
- Adaptive evolution of the mouse CENP-T HFD reduces its centromere binding
- Reduced centromere binding is independent of the centromeric DNA sequence
- Reversing adaptive evolution of the CENP-T HFD decreases oocyte numbers in mice

Authors

Damian Dudka, Alexandra L. Nguyen, Katelyn G. Boese, ..., Ben E. Black, Iain M. Cheeseman, Michael A. Lampson

Correspondence

lampson@sas.upenn.edu

In brief

Dudka et al. reverse adaptive changes in the DNA-binding domain of a centromeric protein, CENP-T. They show that adaptive evolution reduced centromere binding in mice, independent of the centromeric DNA sequence. Their findings suggest adaptation by modulating centromere binding to reduce fitness costs associated with centromere drive.

Dudka et al., 2025, Current Biology *35*, 1–11
March 10, 2025
https://doi.org/10.1016/j.cub.2025.01.017

CellPress

Current Biology

CellPress

Article

Adaptive evolution of CENP-T modulates centromere binding

Damian Dudka,[1] Alexandra L. Nguyen,[2,3] Katelyn G. Boese,[1] Océane Marescal,[2,3] R. Brian Akins,[1] Ben E. Black,[4,5,6] Iain M. Cheeseman,[2,3] and Michael A. Lampson[1,6,7,*]

[1]Department of Biology, School of Arts and Sciences, University of Pennsylvania, Philadelphia, PA 19104, USA
[2]Department of Biology, Massachusetts Institute of Technology, Cambridge, MA 02142, USA
[3]Whitehead Institute for Biomedical Research, Cambridge, MA 02142, USA
[4]Department of Biochemistry and Biophysics, Perelman School of Medicine, University of Pennsylvania, Philadelphia, PA 19104, USA
[5]Epigenetics Institute, University of Pennsylvania, Philadelphia, PA 19104, USA
[6]Penn Center for Genome Integrity, University of Pennsylvania, Philadelphia, PA 19104, USA
[7]Lead contact
*Correspondence: lampson@sas.upenn.edu
https://doi.org/10.1016/j.cub.2025.01.017

SUMMARY

Centromeric DNA and proteins evolve rapidly despite conserved function in mediating kinetochore-microtubule attachments during cell division. This paradox is explained by selfish DNA sequences preferentially binding centromeric proteins to disrupt attachments and bias their segregation into the egg (drive) during female meiosis. Adaptive centromeric protein evolution is predicted to prevent preferential binding to these sequences and suppress drive. Here, we test this prediction by defining the impact of adaptive evolution of the DNA-binding histone fold domain of CENP-T, a major link between centromeric DNA and microtubules. We reversed adaptive changes by creating chimeric variants of mouse CENP-T with the histone fold domain from closely related species, expressed exogenously in mouse oocytes or in a transgenic mouse model. We show that adaptive evolution of mouse CENP-T reduced centromere binding, which supports robust female gametogenesis. However, this innovation is independent of the centromeric DNA sequence, as shown by comparing the binding of divergent CENP-T variants to distinct centromere satellite arrays in mouse oocytes and in somatic cells from other species. Overall, our findings support a model in which selfish sequences drive to fixation, disrupting attachments of all centromeres to the spindle. DNA sequence-specific innovations are not needed to mitigate fitness costs in this model, so centromeric proteins adapt by modulating their binding to all centromeres in the aftermath of drive.

INTRODUCTION

Chromosome segregation is a widely conserved process mediated by centromeres, which are specialized chromatin regions composed of centromeric DNA and centromeric proteins. Centromeric proteins recruit multi-protein kinetochore complexes that bind spindle microtubules to segregate chromosomes.[1,2] To ensure accurate segregation, centromeres also recruit proteins that destabilize erroneous microtubule-binding attachments.[3,4] These essential functions of centromeric proteins have been defined by studies focused exclusively on conserved regions[2,5,6] of their ancient domains, retained over long evolutionary timescales.[7] However, many of these domains show signs of rapid evolution via positive selection, detected in computational analyses as increased amino acid divergence between closely related species,[8,9] suggesting evolutionary innovations.[10–17] Although protein innovations have been shown to bring about adaptation to environmental changes,[18] viral infections[19] or transposable elements,[20] their role in centromere biology remains poorly defined.

The leading explanation for the rapid evolution of centromeric proteins is their co-evolution with centromeric DNA, which is composed of highly repetitive and ever-changing DNA satellites.[21] Centromeric proteins may simply adapt by increasing binding to new satellites to preserve robust kinetochore-microtubule attachments. Alternatively, the "centromere drive" hypothesis proposes that centromeric proteins adapt to "selfish" DNA sequences[11] that emerge at centromeres, which compete for inheritance during the asymmetric female meiotic division. According to this hypothesis, selfish sequences bias their segregation to the egg (drive) by binding more centromeric proteins compared with centromeres of the homologous chromosomes, which segregate instead to the degenerating polar body and are lost (Figure 1A). Fitness costs of this selfish behavior, such as chromosome segregation errors, would select for rapid amino acid changes in DNA-binding centromeric proteins. Those changes are predicted to prevent preferential protein binding to selfish DNA sequences, thus restoring protein balance across centromeres of homologous chromosomes and suppressing drive.[11,22,23] The emergence of new selfish DNA sequences would require new innovations, consistent with the observed

Please cite this article in press as: Dudka et al., Adaptive evolution of CENP-T modulates centromere binding, Current Biology (2025), https://doi.org/10.1016/j.cub.2025.01.017

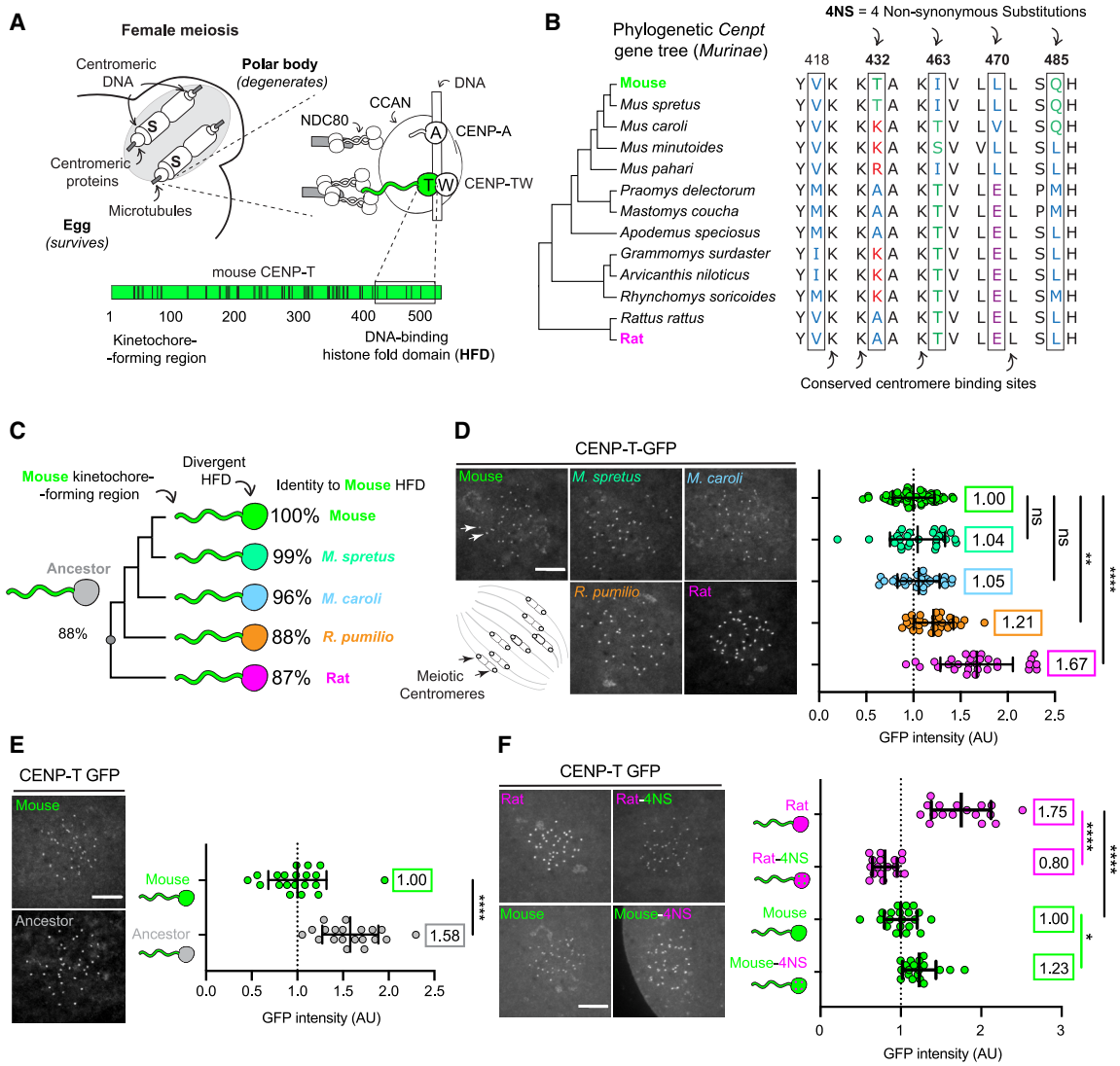

Figure 1. Evolutionary innovation in the mouse CENP-T HFD reduced its centromere binding

(A) Selfish centromeric DNA sequences (S) bias their segregation into the egg during female meiosis I by recruiting more centromeric proteins than centromeres of homologous chromosomes that segregate into the degenerating polar body (left). CENP-A and CENP-T directly bind centromeric DNA and recruit kinetochore proteins. For simplicity, only centromeric proteins CENP-A, CENP-T, and CENP-W and the microtubule-binding kinetochore NDC80 complex are depicted. CCAN, constitutive centromere-associated network. CENP-W is an obligatory CENP-T binding partner (right). Green bar shows sites with signatures of positive selection in *Murinae* CENP-T (black lines).

(B) Recurrent amino acid changes across 13 *Murinae* species at 5 sites (black boxes) with signatures of positive selection in the CENP-T HFD. Clustal color scheme highlights residue types. Arrows show residues swapped in (F) (4NS; top) and conserved sites (bottom).

(C) CENP-T constructs include the kinetochore-forming N terminus from mouse CENP-T, with HFDs from the indicated species.

(D–F) Images show metaphase I mouse oocytes expressing GFP-tagged mouse CENP-T or chimeric variants with HFDs from other species (D), matching color scheme in (C), the predicted HFD from the ancestor of mouse and rat (E), the mouse HFD with rat-specific mutations in recurrently changing residues (top arrows in B), or the rat HFD with mouse-specific mutations in the same residues (F). Scale bars, 10 μm. Arrows (D) indicate centromeres of paired homologous chromosomes, as shown in the schematic. Graphs show GFP intensity at centromeres, normalized to control mouse CENP-T-GFP. Each dot represents centromeres averaged over one cell, and bars show means and standard deviations, means in boxes, $n = 28–59$ cells from 3 independent experiments (D) or 17–20 cells from 2 independent experiments (E and F) for each construct; one-way ANOVA with Tukey's multiple comparison test (D and F) or unpaired two-tailed t test (E), $^{*}p < 0.05$, $^{**}p < 0.01$, $^{****}p < 0.0001$, ns: not significant.

See also Figures S1 and S3.

recurrent amino acid changes over short evolutionary timescales.[10,12,15–17] Indeed, experimental studies in monkeyflowers and mouse oocytes provided evidence that centromeric DNA can drive[24–27] and elicit a fitness cost.[25,28] Work in mouse oocytes showed that selfish centromeres drive by disrupting kinetochore-microtubule attachments,[27,29,30] suggesting that drive increases the chance of chromosome mis-segregation. However, while the centromere drive hypothesis was inspired

Please cite this article in press as: Dudka et al., Adaptive evolution of CENP-T modulates centromere binding, Current Biology (2025), https://doi.org/10.1016/j.cub.2025.01.017

by the rapid evolution of centromeric proteins,[11] which is widespread,[10–12,14–17,31–33] the functional impacts of this protein evolution remain to be tested.

Mouse oocytes are currently the only experimentally tractable model of centromere drive.[16,26,27,29,30,34] Our computational analyses of rodents that span mouse and rat (*Murinae*)[16,17] revealed that many rodent centromeric proteins evolve adaptively. We selected centromere protein T (CENP-T) as an ideal candidate for functional studies because it directly binds centromeric DNA, regulates kinetochore-microtubule attachments, and shows signatures of positive selection near functionally important sites. CENP-T recruits the microtubule-binding nuclear division cycle 80 (NDC80) complex[35–39] and directly binds centromeric DNA via its histone fold domain (HFD; Figure 1A).[40–42] Critically, the CENP-T HFD contains residues with signatures of positive selection next to highly conserved sites known to regulate its centromeric localization[16,17,40] (Figure 1B). Here, we used mouse oocytes, somatic cells, and transgenic mice to define the impact of putative evolutionary innovation in the mouse CENP-T HFD on centromere binding.

RESULTS

Evolutionary innovation in the mouse CENP-T HFD reduced its centromere binding

To test if adaptive evolution shapes centromere binding, we created chimeric mouse CENP-T variants with the DNA-binding HFDs from closely related species. This evolution-guided approach creates an evolutionary mismatch between *Mus musculus* (mouse) centromeric DNA and the CENP-T HFD of divergent species, revealing potential functional differences due to amino acid changes that occurred naturally over short evolutionary timescales (Figure S1A) while minimizing the probability of loss-of-function mutations.[20] Given that the swapped domain is fully functional in a related species, severe phenotypic changes typical for conventional null mutations are unlikely. We expressed GFP-tagged chimeras from species either most closely related to mouse (*M. spretus* and *M. caroli*) or more divergent (*Rhabdomys pumilio* and *Rattus norvegicus* [rat]) (Figure 1C), at comparable levels in mouse oocytes (Figure S1B), and measured centromere localization. We anticipated that if mouse HFD evolved to maintain robust interactions with changing DNA satellites, mouse CENP-T would show higher centromere binding compared with chimeric CENP-T variants. Contrary to this prediction, we observed lower binding of mouse CENP-T compared with variants with more divergent HFDs (Figure 1D). Since divergent CENP-T HFDs could not have evolved to strongly bind to mouse centromeres, these results suggest that evolutionary changes in mouse CENP-T reduced its binding to its own centromeres. To test this idea further, we reversed the amino acid changes that have accumulated in the CENP-T HFD since the common ancestor of mouse and rat, leveraging a widely used molecular evolution tool (see STAR Methods). This resurrected HFD also showed increased binding to mouse centromeres compared with mouse CENP-T (Figures 1E and S1C), corroborating that mouse CENP-T evolved to reduce centromere binding over short evolutionary timescales.

If reduced centromere binding is an evolutionary innovation of mouse CENP-T HFD, we expected it to be mediated by residues with statistical signatures of positive selection. We focused on the CENP-T variant with the rat HFD (hereafter "chimeric CENP-T"), which shows the strongest centromere binding in our assay (Figure 1D). Specifically, we swapped 4 such positively selected residues in the rat HFD to those found in mouse ("4NS"; Figure 1B). Conversely, we swapped the corresponding residues in the mouse HFD to those found in rat. The mouse-specific residues reduced chimeric CENP-T centromere binding, while the rat-specific residues increased mouse CENP-T binding (Figures 1F and S1D). The more modest increase seen with rat-specific residues, as compared with the entire rat HFD, suggests that epistatic interactions that potentiate centromere binding of rat HFD are absent in the mouse domain. Overall, these analyses indicate that positively selected mouse residues in the HFD mediate reduced centromere binding.

Organismal impact of evolutionary innovation in the mouse CENP-T HFD

If reduced centromere binding of the mouse CENP-T HFD is adaptive, the absence of that innovation should have functional consequences for the organism. To test this prediction, we modified the endogenous mouse CENP-T allele to generate a mouse model with a chimeric CENP-T. We swapped exons encoding the mouse CENP-T HFD with those from rat and retained rat introns to avoid disrupting splicing sites (Figures 2A and S2A). The *Cenpt* allele was not modified in any other way, minimizing the likelihood of a hypomorphic allele, and ensuring that any phenotypic changes are due to the amino acid sequence divergence between mouse and rat. We observed increased levels of endogenous chimeric CENP-T at centromeres in oocytes (Figure 2B), albeit more subtle than in overexpression experiments (Figure 1D), possibly due to mechanisms regulating kinetochore size *in vivo* during early embryo development or in the female germ line.[43] We then tested organismal impact by two widely used general metrics of fitness: viability and fertility[20] (Figure S2B), recognizing that fitness impacts with large effect at evolutionary timescales[44] are challenging to capture in a laboratory setting. We did not observe significant differences in viability (Figure 2C), but females homozygous for the chimeric allele produced significantly fewer oocytes (Figure 2D). This impact on female fertility was not detectable by measuring litter sizes (Figure S2C), which are highly variable, given limited sample sizes inherent to mouse models. We did not detect significant differences in the number of sperm or in testis weight from homozygous chimeric CENP-T males (Figures 2E and S2D), indicating that chimeric CENP-T is associated primarily with disrupted oogenesis. Evolutionary innovation of mouse CENP-T therefore supports the robust production of female gametes, although the mechanisms underlying such sex-specific sensitivity remain to be determined.

Evidence of evolutionary innovation in interactions between CENP-T and CENP-W

Conspecific binding partners facilitate centromere binding of CENP-A, another key centromeric protein, which evolves adaptively in flies and plants[13,45,46] (Figure 1A). In vertebrates, CENP-T centromere binding requires dimerization of its HFD

Please cite this article in press as: Dudka et al., Adaptive evolution of CENP-T modulates centromere binding, Current Biology (2025), https://doi.org/10.1016/j.cub.2025.01.017

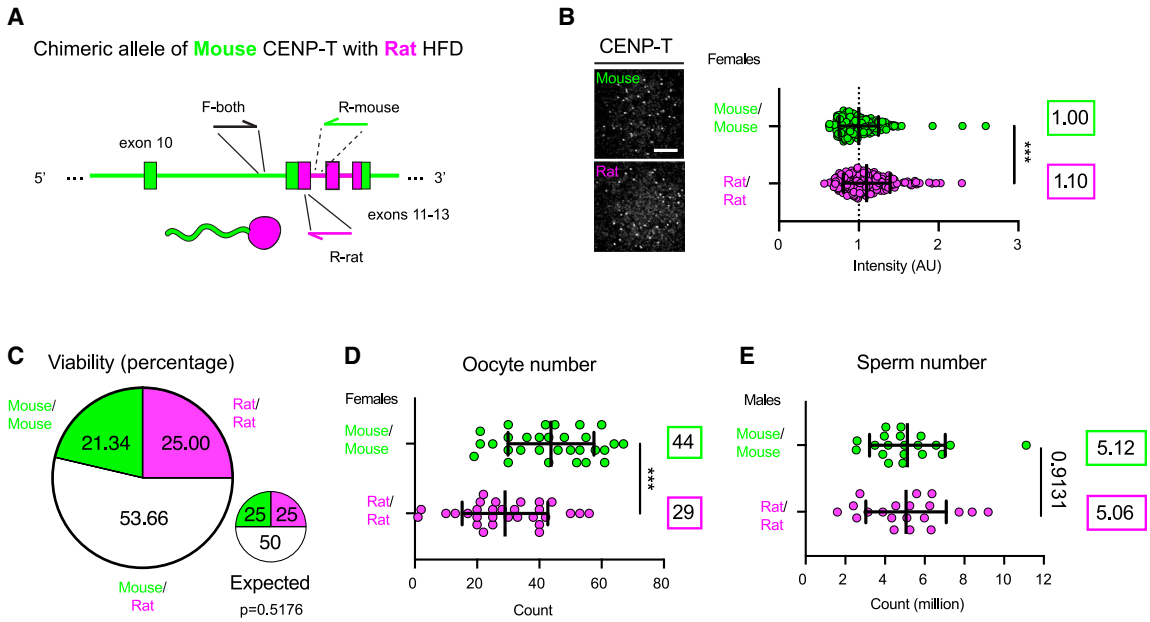

Figure 2. Organismal impact of evolutionary innovation in the mouse CENP-T HFD

(A) Chimeric allele topology showing the swapped region corresponding to the HFD (413–503 aa) and genotyping primers.

(B) Metaphase I oocytes from females homozygous for mouse CENP-T or chimeric CENP-T (with the rat HFD) were fixed and stained for endogenous CENP-T. Graph shows CENP-T intensity at centromeres, normalized to mouse CENP-T. Each dot represents centromeres averaged over one cell, and bars show means and standard deviations, means in boxes, n = 187–222 oocytes from 25 to 27 females from 10 independent experiments; two-tailed Mann-Whitney test, ***$p < 0.001$. Scale bars, 10 μm. Note that those experiments include control data shown in Figure 3E.

(C) Viability assay: genotype frequencies of progeny from heterozygous parents were compared with the expected 25:50:25 ratio; n = 24 litters from 10 pairs; 164 pups; chi-square test.

(D) Count of mature oocytes dissected from both ovaries after superovulation of homozygous females. Each dot represents a single female, and bars show means and standard deviations, means in boxes, n = 30 females per genotype; unpaired two-tailed t test, ***$p < 0.001$.

(E) Sperm count from each epididymis of homozygous males. Each dot represents the average number of sperm per testis, and bars show means and standard deviations, means in boxes, n = 10 males per genotype (20 testes); unpaired two-tailed t test.

See also Figure S2.

with the obligatory binding partner CENP-W[40,41] (Figure 1A). Given the high conservation of the CENP-T-HFD:CENP-W dimer[40,42,47] (Figure 3A), we anticipated that even small changes in CENP-T HFD conformation could impact interactions with CENP-W. To capture subtle evolutionary changes before dimerization, we used monomer modeling with evolutionary scale modeling fold (ESMFold),[48] which generates accurate predictions with sensitivity to single amino acid substitutions.[49,50] Superposition of the predicted mouse and rat CENP-T HFDs shows two inward shifts in the rat HFD of α1 and α5 helices that contact the CENP-W central helix (Figure 3B). Moreover, mouse-specific residues that have evolved under positive selection are sufficient to abolish the shift of the α5 helix in the rat HFD (Figure 3C), whereas rat-specific residues induce this shift in the mouse HFD (Figure 3D). The predicted conformation changes correlate with the centromeric recruitment of those CENP-T variants (Figure 1F). Consistently, we observed similar inward shifts of the ancestral or *R. pumilio* HFDs (Figure S3), which also show stronger centromere binding compared with the mouse HFD (Figures 1D and 1E). Since our modeling reflects a conformation that the CENP-T HFD could adopt in solution before encountering CENP-W, we propose that adaptive changes in mouse CENP-T modulate interactions with CENP-W to reduce centromere binding.

The structure predictions motivated our hypothesis that increased centromere binding of the chimeric CENP-T (with the rat HFD, Figures 1D and 2B) reflects its increased binding to mouse CENP-W. We leveraged our transgenic mouse model with endogenous chimeric CENP-T, in comparison to wild-type animals with endogenous mouse CENP-T, to examine changes in centromere binding induced by excess mouse CENP-W. We found that mouse CENP-W overexpression increased the level of CENP-T at centromeres in oocytes expressing endogenous mouse CENP-T more than in oocytes expressing endogenous chimeric CENP-T (35% increase for mouse CENP-T vs. 14% increase for chimeric CENP-T; Figures 3E and S4). This observation suggests that most of the chimeric CENP-T is already bound by endogenous mouse CENP-W, so additional mouse CENP-W has little effect on centromere binding. Conversely, a smaller fraction of mouse CENP-T is bound by endogenous mouse CENP-W, consistent with lower affinity for CENP-W. Consequently, additional mouse CENP-W leads to increased formation of dimers with mouse CENP-T and increased centromere binding. Addition of rat CENP-W does not increase either mouse or chimeric CENP-T at centromeres (Figure S5). This result suggests a mild cross-species incompatibility between rat CENP-W and mouse centromeres and is consistent with the idea that chimeric CENP-T is already bound

Please cite this article in press as: Dudka et al., Adaptive evolution of CENP-T modulates centromere binding, Current Biology (2025), https://doi.org/10.1016/j.cub.2025.01.017

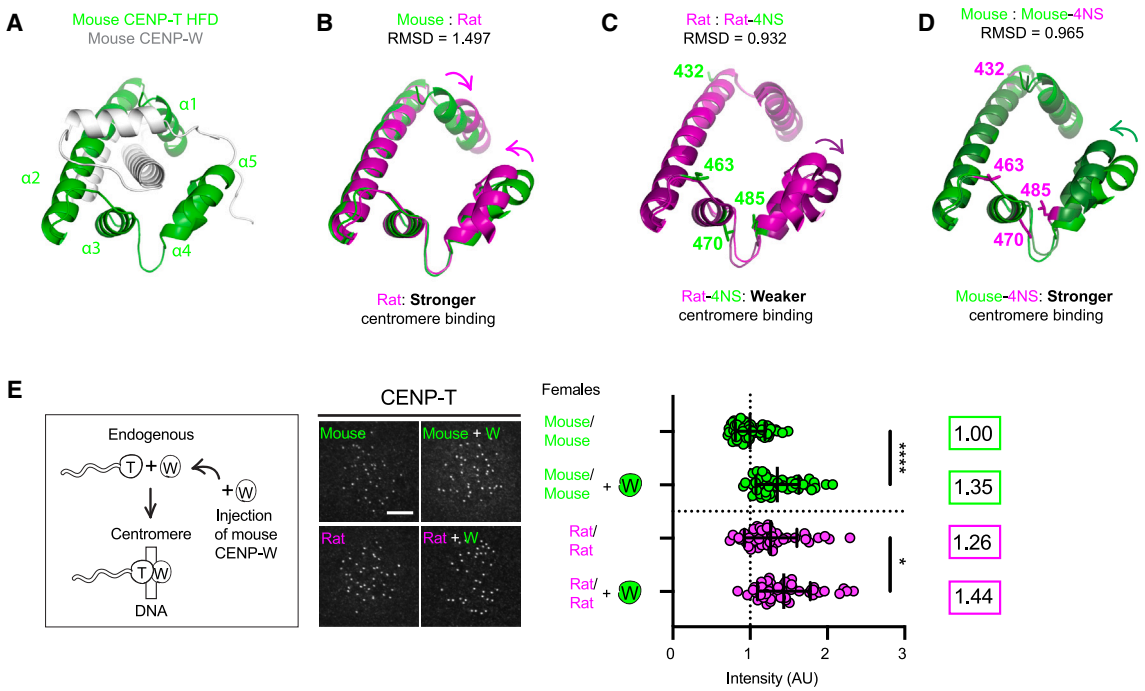

Figure 3. Evidence of evolutionary innovation in interactions between CENP-T and CENP-W

(A) ESMFold structure prediction shows the mouse CENP-T HFD (green) enclosing the central helix of CENP-W (gray). The last 12 residues (histone fold extension) are not depicted for clarity.

(B–D) Superpositions of CENP-T HFD structure predictions: rat vs. mouse (B), rat vs. rat-4NS (C), or mouse vs. mouse-4NS (D). Root-mean-square deviation (RMSD) indicates the difference between the two structures. Arrows show conformation shifts in α1 (upper) and α5 (bottom) helices. The relative effect on centromere binding reported in Figure 1F is indicated.

(E) Schematic shows the experimental setup. Mouse oocytes from females homozygous for the mouse or chimeric (rat HFD) CENP-T allele were injected with water (control) or RNA encoding mouse CENP-W. Cells were fixed at metaphase I and stained for endogenous CENP-T. Scale bar, 10 μm. Graph shows CENP-T intensity at centromeres, normalized to control mouse CENP-T. Each dot represents centromeres averaged over one cell, and bars show means and standard deviations, means in boxes, n = 48–63 oocytes from 4 independent experiments; Kruskal-Wallis with Dunn's multiple comparison test, $^{****}p < 0.0001$, $^{*}p < 0.05$. See also Figures S3–S5.

by endogenous mouse CENP-W. Together, our structural modeling and experimental results support the idea that changes in interactions with CENP-W contribute to evolutionary innovations in the CENP-T HFD.

Evolutionary innovation of the mouse CENP-T HFD is DNA sequence independent

The current centromere drive model predicts that DNA-binding centromeric proteins evolve to suppress biased segregation in female meiosis by reducing preferential binding to selfish centromeric DNA sequences.[11,23] We determined if evolution to reduce centromere binding of the mouse CENP-T HFD depends on the underlying centromeric DNA sequence using two parallel approaches. First, we measured binding of GFP-tagged CENP-T variants to two divergent DNA satellites adjacent to one another at mouse centromeres: minor satellite (centromere) and major satellite (pericentromere).[51] We leveraged our ability to spatially separate the two satellites in mouse oocytes via acute depletion of the major satellite-packaging high mobility group A1 (HMGA1) protein[52] (Figures 4A and 4B). We found that mouse CENP-T was present only at minor satellite (marked by NDC80; Figures 4C and 4D), consistent with supporting kinetochore formation as part of the CENP-A-associated centromere network[26,42,47,53] (Figure 1A), which is specific to the minor satellite in mice.[26,51,54] By contrast, chimeric CENP-T bound to both minor and major satellites (DNA stretches; Figures 4C and 4E). If evolution of the mouse CENP-T HFD depended on the centromeric DNA sequence, then chimeric CENP-T with 4 mouse-specific residues (4NS) should reduce binding to only the minor satellite. Instead, we found that both minor and the major satellite populations of CENP-T were reduced (Figures 4C–4F), indicating that adaptive evolution of mouse CENP-T to reduce centromere binding does not depend on a specific centromeric DNA sequence.

Second, we further assessed sequence-dependent innovation of mouse CENP-T by testing its binding to more divergent centromeric satellites using somatic cells of different species. We expressed the same GFP-tagged CENP-T variants in mouse, rat, and human cells, which have completely different centromeric satellites.[55] We observed increased centromere binding of chimeric CENP-T relative to mouse CENP-T in all cases (Figures 4G–4I), consistent with the results in mouse oocytes (Figures 1D and 2B). Mouse-specific residues also reduced chimeric CENP-T binding to centromeres in all species (Figures 4G–4I), consistent with DNA sequence-independent reduction of centromere binding. We conclude that evolutionary

Please cite this article in press as: Dudka et al., Adaptive evolution of CENP-T modulates centromere binding, Current Biology (2025), https://doi.org/10.1016/j.cub.2025.01.017

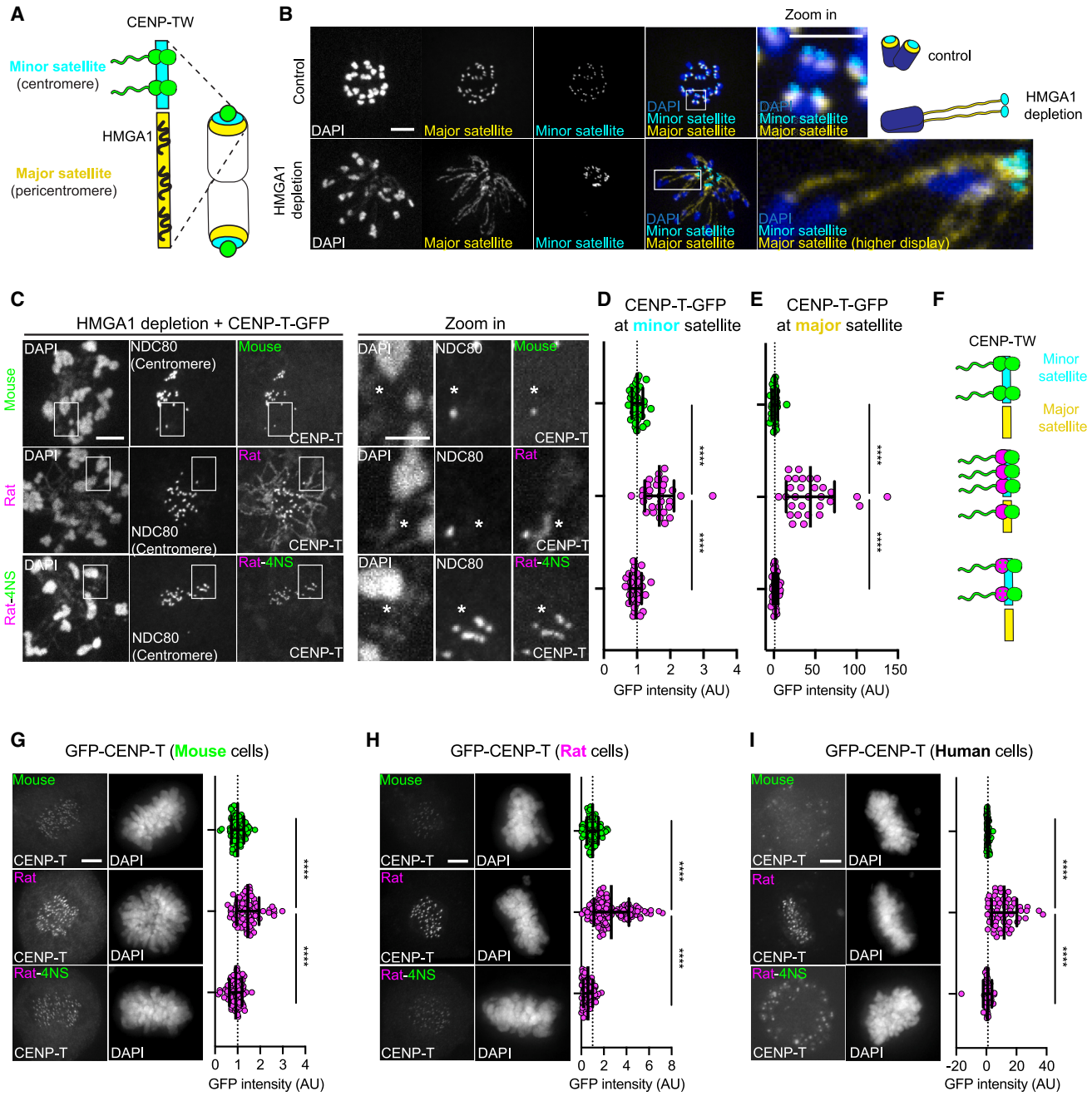

Figure 4. Evolutionary innovation of the mouse CENP-T HFD is DNA sequence independent

(A) Centromeric minor satellite in mice (cyan) and the adjacent pericentromeric major satellite (yellow) organized by HMGA1 (black).

(B) Acute HMGA1 depletion in mouse oocytes unpackages the major satellite, displacing the minor satellite from chromosome arms (dark blue in schematic). Cells were expressing transcription activator-like effector (TALE)-mClover targeting major satellite and dCas9-mCherry in complex with guide RNA targeting minor satellite. Scale bars, 5 (insets) or 10 μm.

(C) Acute HMGA1 depletion in mouse oocytes expressing CENP-T-GFP variants: mouse, chimeric with the rat HFD, or with the rat HFD with mouse-specific mutations in recurrently changing residues (4NS). Boxed regions are magnified on the right, with asterisks marking DNA stretches corresponding to major satellite. Scale bars, 10 μm.

(D and E) Average CENP-T-GFP signal at centromeres (D) or pericentromeres (E). Each dot represents a single cell, and bars show means and standard deviations, $n = 29–30$ oocytes from 3 independent experiments; Kruskal-Wallis with Dunn's multiple comparison test, $^{****}p < 0.0001$, ns: not significant.

(F) Mouse-specific residues reduce chimeric CENP-T-GFP binding at both satellites.

(G–I) GFP-CENP-T variants expressed in mouse (G; NIH3T3), rat (H; Rat2), or human (I; HeLa) somatic cells. Means and standard deviations are indicated, $n = 51–126$ cells from 2 independent experiments; Kruskal-Wallis with Dunn's multiple comparison test, $^{****}p < 0.0001$, ns: not significant.

Please cite this article in press as: Dudka et al., Adaptive evolution of CENP-T modulates centromere binding, Current Biology (2025), https://doi.org/10.1016/j.cub.2025.01.017

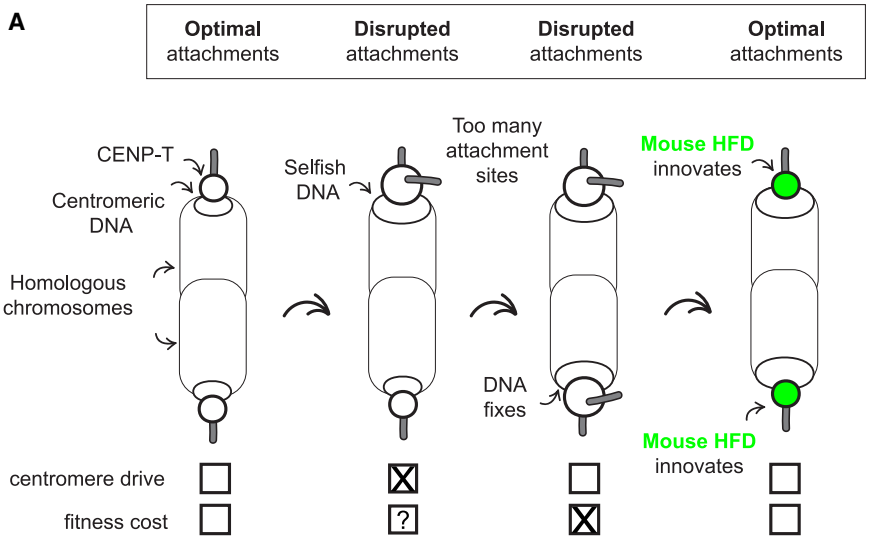

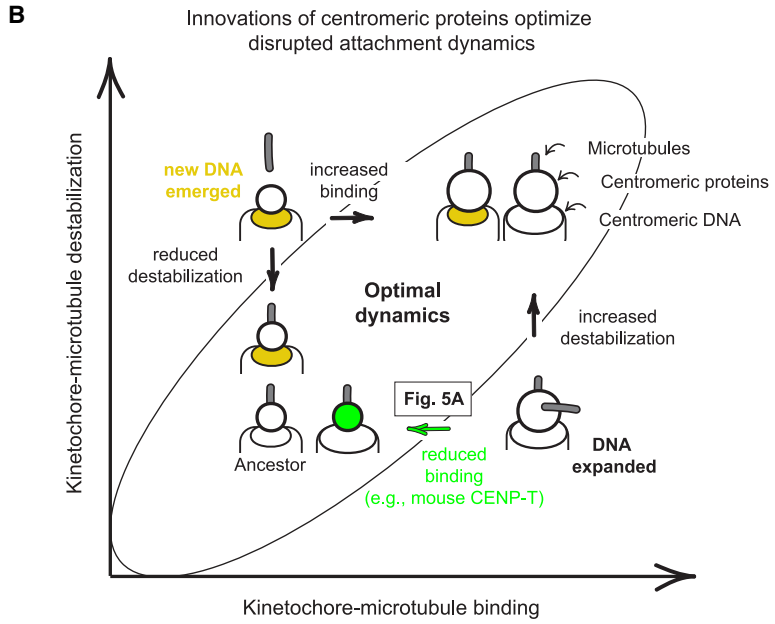

Figure 5. Evolutionary innovations of centromeric proteins in the aftermath of centromere drive

(A) Scenario leading to mouse CENP-T innovation reducing centromere binding. Selfish DNA binds more centromeric proteins than the centromere of the homologous chromosome and drives to fixation. By recruiting too many kinetochore proteins and creating too many microtubule-binding sites, the selfish DNA would disrupt kinetochore-microtubule attachments at all centromeres. Evolutionary innovation in the mouse CENP-T HFD would reduce centromere binding and the number of microtubule-binding sites.

(B) Model for evolutionary innovations in centromeric proteins. Optimal kinetochore-microtubule attachment dynamics (inside ellipse) require a balance between microtubule binding and destabilizing activities. Dynamics can be disrupted by changes in either centromeric DNA amount (e.g., expansion) or sequence. For simplicity, satellite expansion is depicted as changing microtubule binding (i.e., by changing kinetochore size) and new DNA satellite, as recruiting more microtubule-destabilizing proteins (yellow). Protein innovations can restore optimal dynamics by modulating centromere binding of proteins with microtubule-binding (horizontal arrows, e.g., CENP-T in green) or microtubule-destabilizing (vertical arrows) activities.

innovation of the mouse CENP-T HFD is independent of the underlying centromeric DNA sequence.

DISCUSSION

Our evolution-guided study tests a key prediction of the current centromere drive model[11,23]: that centromeric proteins evolve adaptively to reduce preferential binding to selfish DNA sequences during female meiosis. Swapping specific residues that evolved under positive selection in the mouse CENP-T HFD demonstrates their function in reducing centromere binding in mouse oocytes (Figure 1), consistent with adaptive evolution. We also show the impact of that innovation at the organismal level in transgenic mice (Figure 2). Our findings support the current centromere drive model by showing that mouse CENP-T innovated by reducing centromere binding (Figures 1, 2, 3, and 4). However, our results are inconsistent with a core premise of the model because this innovation is independent of the centromeric DNA sequence (Figure 4).

To interpret these findings, we consider what happens when a selfish DNA sequence (either a new sequence or an expansion of a current satellite) first emerges at a single centromere (Figure 5A). By binding more centromeric proteins to disrupt microtubule attachments, selfish DNA initially creates an imbalance across the centromeres of a single pair of homologous chromosomes in female meiosis, leading to centromere drive. To restore balance and suppress drive, DNA-binding centromeric proteins could evolve to reduce preferential binding to the selfish sequence,[11,23] but experimental evidence of such innovation remains elusive. Alternatively, centromere-adjacent heterochromatin proteins may evolve to become a dominant pathway regulating attachments, thus restoring balance by minimizing the contribution of selfish centromeric DNA.[16] In these scenarios, centromeric proteins need to adapt before the selfish centromeric DNA sequence drives to fixation (by outcompeting centromeres of homologous chromosomes). While work in monkeyflowers showed that a single amino acid change in CENP-A occurred before fixation of the selfish

Please cite this article in press as: Dudka et al., Adaptive evolution of CENP-T modulates centromere binding, Current Biology (2025), https://doi.org/10.1016/j.cub.2025.01.017

centromeric D locus,[56] the functional impact of that change on CENP-A function and drive suppression remains to be tested. We propose that rather than suppressing drive, centromeric proteins evolve to mitigate deleterious consequences in the aftermath of drive. Selfish DNA may invade other centromeres (e.g., via recombination, transposition,[57] or structural rearrangements[21]) and quickly drive to fixation, consistent with the observation that centromere sequences are similar within species but diverged between species.[58–61] Attachments would then be disrupted at all centromeres. In mice, our finding that CENP-T innovated by reducing centromere binding suggests that selfish DNA disrupted attachments by making large kinetochores with too many microtubule-binding sites, increasing chromosome mis-segregation.[62] With selfish DNA present at all centromeres, selection would no longer favor DNA sequence-specific innovations. Instead, centromeric proteins would evolve to mitigate the costs associated with disrupted attachments at all centromeres, for example, by reducing kinetochore size in the case of mouse CENP-T. Consistent with this model, we find that positively selected residues modulate CENP-T centromere binding independent of the DNA sequence. Furthermore, this model accounts for the longer time needed to accumulate beneficial mutations in protein-coding sequences, as compared with much more rapid satellite DNA changes.[21]

Although rooted in the centromere drive hypothesis, our model applies to any changes in centromeric DNA that disrupt kinetochore-microtubule attachments at all centromeres (Figure 5B). Centromere function depends on a balance of microtubule-binding and microtubule-destabilizing activities.[3] We propose that these dynamics are recurrently disrupted by rapid changes in the satellite DNA, including the emergence of new selfish sequences and changes in the amount of the current satellite (expansions or contractions). Therefore, mutations in centromeric proteins that restore the optimal dynamics will be favored, regardless of whether those proteins interact directly with the DNA. Potential targets of selection include proteins that modulate the number of microtubule-binding sites (e.g., CENP-T, CENP-A,[10,12–17,31–33,47,63,64] CENP-I,[10,12–17,31–33,47,63,64] CENP-L,[10,12–17,31–33,47,63,64] CENP-Q,[10,12–17,31–33,47,63,64] and CENP-U[10,12–17,31–33,47,63,64]) or promote microtubule destabilization (e.g., Kif2b,[17] INCENP[16,17], Haspin,[16,17] and Aurora C[17,33]). Evolutionary innovation in centromere binding of CENP-T, which directly recruits the microtubule-binding NDC80 complex,[35–39] is consistent with this model. We infer that swapping the mouse CENP-T HFD to the one optimized in rat shifts the dynamics outside of the optimal range for mouse centromeres, consistent with deleterious consequences in the mouse female germ line (Figure 2).

Based on our chimeric CENP-T mouse model, female gametogenesis emerges as a process sensitive to changes in kinetochore-microtubule attachment dynamics. A reduced number of oocytes (which are arrested in prophase of meiosis I) suggests a vulnerability of pre-meiotic divisions in the female germ line to changes in CENP-T (Figure 2). Indeed, asymmetric divisions of both female and male germline stem cells are sensitive to kinetochore size in flies.[65–68] Although both types of gametes form in cysts of inter-connected cells across the animal kingdom,[69,70] only a few of the female stem cells will become oocytes, which depends on the flow of cytoplasmic content from nurse cells into the oocyte through inter-cellular bridges.[71] Therefore, one explanation for a female-specific vulnerability is disrupted formation or maintenance of these bridges due to defects in pre-meiotic divisions in the cyst in chimeric mice. Another possibility is the increase in centromere size reported recently in the female germ line,[43] suggesting that additional increase by recruiting more CENP-T would exceed an optimal number of microtubule-binding sites in chimeric oocytes. Germline stem cell divisions may be a common vulnerability of disrupted attachment dynamics, as monkeyflowers homozygous for an expanded selfish centromeric satellite produce fewer gametes, albeit in both females[28] and males.[25] Testing this idea will be an important avenue for future research.

Finally, our findings suggest a mechanism underlying DNA sequence-independent innovation in mouse CENP-T. We propose that changes in binding affinity for CENP-W regulate the concentration of the CENP-TW complex that can be recruited to centromeres. This idea is consistent with the presence of recurrently changing residues next to a conserved site that mediates complex formation (L471).[40] We speculate that mouse CENP-T HFD monomers adopt a more flexible conformation, reducing binding affinity to CENP-W. Reduced centromere binding of mouse CENP-T compared with chimeric CENP-T expressed in other species suggests that such flexibility reduces affinity to any CENP-W, consistent with high conservation of the CENP-TW dimer conformation.[40,42,47] Reducing the amount of the complex may restrict its localization to sites where binding to centromeric satellites is facilitated by CENP-A-associated CENP-LN and CENP-HIKM complexes,[72,73] rather than less favored sites at the pericentromere. Another possible mechanism for DNA sequence-independent innovation is that residues that evolved under positive selection modulate binding to a common feature of the centromeric chromatin, e.g., non-B form DNA,[74] methylated DNA,[75] or a histone post-translational modification.[76] Consistently, moth CENP-T recognizes transcriptionally silent chromatin rather than a particular DNA sequence.[77] Together, our evolution-guided approaches pave the way for experimental studies of how evolutionary innovations ensure faithful chromosome segregation in the face of rapidly changing centromeric DNA.

RESOURCE AVAILABILITY

Lead contact

Further information and requests for resources and reagents should be directed to and will be fulfilled by the lead contact, Michael A. Lampson (lampson@sas.upenn.edu).

Materials availability

Further information and requests for resources and reagents should be directed to and will be fulfilled by Michael A. Lampson (lampson@sas.upenn.edu). Transgenic mice generated in this manuscript will be cryopreserved and available upon request. Plasmids generated in this study will be available from Addgene (Michael Lampson Lab Plasmids).

Data and code availability

- All the data reported in this paper will be shared by the lead contact, Michael A. Lampson (lampson@sas.upenn.edu), upon request.
- This paper does not report original code.
- Any additional information required to reanalyze the data reported in this work paper is available from the lead contact upon request.

ACKNOWLEDGMENTS

This research was funded by the Swiss National Science Foundation post-doctoral fellowship P2GEP3_187772 awarded to D.D., the Damon Runyon post-doctoral fellowship awarded to A.L.N., the National Science Foundation grant 2029868 and National Institutes of Health grant R35GM126930 awarded to I.M.C., and the National Institutes of Health grant R35GM122475 awarded to M.A.L. We would like to thank all the members of the Lampson and Levine labs (University of Pennsylvania) and members of the Philadelphia Chromosome Club for discussing the data. Special thanks to Mia Levine and Cara Brand (both University of Pennsylvania) for critical reading of the manuscript, Frances Hauser (University of Toronto) for help with ancestral CENP-T reconstruction, Eszter Posfai (Princeton University) for data discussion and suggestions, and Keagan Beeravolu (University of Pennsylvania) for help with genotyping.

AUTHOR CONTRIBUTIONS

Conceptualization, D.D. and M.A.L.; formal analysis, D.D., A.L.N., and K.G.B.; methodology, D.D., A.L.N., and K.G.B.; investigation, D.D., A.L.N., and K.G.B.; visualization, D.D. and A.L.N.; funding acquisition, D.D., A.L.N., I.M.C., and M.A.L.; project administration, D.D. and M.A.L.; supervision, D.D., A.L.N., I.M.C., and M.A.L.; resources, O.M., B.E.B., I.M.C., and M.A.L.; software, R.B.A.; writing – original draft, D.D.; writing – review and editing, D.D., A.L.N., K.G.B., R.B.A., B.E.B., I.M.C., and M.A.L.

DECLARATION OF INTERESTS

The authors declare no competing interests.

STAR★METHODS

Detailed methods are provided in the online version of this paper and include the following:

- KEY RESOURCES TABLE
- EXPERIMENTAL MODEL AND STUDY PARTICIPANT DETAILS
  - Mice
  - Cell lines
- METHOD DETAILS
  - Plasmid generation
  - Retrovirus preparation and transduction
  - Antibody generation
  - Oocyte collection and microinjection
  - Sperm collection
  - Image acquisition: oocytes
  - Image acquisition: Somatic cells
  - Image analysis
  - Molecular evolution analyses
  - Structure modeling
- QUANTIFICATION AND STATISTICAL ANALYSIS

SUPPLEMENTAL INFORMATION

Supplemental information can be found online at https://doi.org/10.1016/j.cub.2025.01.017.

Received: August 16, 2024
Revised: November 19, 2024
Accepted: January 13, 2025
Published: February 12, 2025

REFERENCES

1. Kixmoeller, K., Allu, P.K., and Black, B.E. (2020). The centromere comes into focus: from CENP-A nucleosomes to kinetochore connections with the spindle. Open Biol. *10*, 200051. https://doi.org/10.1098/rsob.200051.
2. McKinley, K.L., and Cheeseman, I.M. (2016). The molecular basis for centromere identity and function. Nat. Rev. Mol. Cell Biol. *17*, 16–29. https://doi.org/10.1038/nrm.2015.5.
3. Godek, K.M., Kabeche, L., and Compton, D.A. (2015). Regulation of kinetochore-microtubule attachments through homeostatic control during mitosis. Nat. Rev. Mol. Cell Biol. *16*, 57–64. https://doi.org/10.1038/nrm3916.
4. Lampson, M.A., and Grishchuk, E.L. (2017). Mechanisms to avoid and correct erroneous kinetochore-microtubule attachments. Biology (Basel) *6*, 1. https://doi.org/10.3390/biology6010001.
5. Musacchio, A., and Desai, A. (2017). A molecular view of kinetochore assembly and function. Biology (Basel) *6*, 5. https://doi.org/10.3390/biology6010005.
6. Kitajima, T.S. (2018). Mechanisms of kinetochore-microtubule attachment errors in mammalian oocytes. Dev. Growth Differ. *60*, 33–43. https://doi.org/10.1111/dgd.12410.
7. Tromer, E.C., van Hooff, J.J.E., Kops, G.J.P.L., and Snel, B. (2019). Mosaic origin of the eukaryotic kinetochore. Proc. Natl. Acad. Sci. USA *116*, 12873–12882. https://doi.org/10.1073/pnas.1821945116.
8. Pond, S.L.K., Frost, S.D.W., and Muse, S.V. (2005). HyPhy: hypothesis testing using phylogenies. Bioinformatics *21*, 676–679. https://doi.org/10.1093/bioinformatics/bti079.
9. Yang, Z. (2007). PAML 4: phylogenetic analysis by maximum likelihood. Mol. Biol. Evol. *24*, 1586–1591. https://doi.org/10.1093/molbev/msm088.
10. Malik, H.S., and Henikoff, S. (2001). Adaptive evolution of Cid, a centromere-specific histone in Drosophila. Genetics *157*, 1293–1298. https://doi.org/10.1093/genetics/157.3.1293.
11. Henikoff, S., Ahmad, K., and Malik, H.S. (2001). The centromere paradox: stable inheritance with rapidly evolving DNA. Science *293*, 1098–1102. https://doi.org/10.1126/science.1062939.
12. Malik, H.S., Vermaak, D., and Henikoff, S. (2002). Recurrent evolution of DNA-binding motifs in the Drosophila centromeric histone. Proc. Natl. Acad. Sci. USA *99*, 1449–1454. https://doi.org/10.1073/pnas.032664299.
13. Cooper, J.L., and Henikoff, S. (2004). Adaptive evolution of the histone fold domain in centromeric histones. Mol. Biol. Evol. *21*, 1712–1718. https://doi.org/10.1093/molbev/msh179.
14. Talbert, P.B., Bryson, T.D., and Henikoff, S. (2004). Adaptive evolution of centromere proteins in plants and animals. J. Biol. *3*, 18. https://doi.org/10.1186/jbiol11.
15. Schueler, M.G., Swanson, W., Thomas, P.J., NISC; Comparative; Sequencing Program, and Green, E.D. (2010). Adaptive evolution of foundation kinetochore proteins in primates. Mol. Biol. Evol. *27*, 1585–1597. https://doi.org/10.1093/molbev/msq043.
16. Kumon, T., Ma, J., Akins, R.B., Stefanik, D., Nordgren, C.E., Kim, J., Levine, M.T., and Lampson, M.A. (2021). Parallel pathways for recruiting effector proteins determine centromere drive and suppression. Cell *184*, 4904–4918.e11. https://doi.org/10.1016/j.cell.2021.07.037.
17. Dudka, D., Akins, R.B., and Lampson, M.A. (2023). FREEDA: an automated computational pipeline guides experimental testing of protein innovation. J. Cell Biol. *222*, e202212084. https://doi.org/10.1083/jcb.202212084.
18. Eizirik, E., and Trindade, F.J. (2021). Genetics and evolution of mammalian coat pigmentation. Annu. Rev. Anim. Biosci. *9*, 125–148. https://doi.org/10.1146/annurev-animal-022114-110847.
19. Tenthorey, J.L., Emerman, M., and Malik, H.S. (2022). Evolutionary landscapes of host-virus arms races. Annu. Rev. Immunol. *40*, 271–294. https://doi.org/10.1146/annurev-immunol-072621-084422.
20. Brand, C.L., and Levine, M.T. (2021). Functional diversification of chromatin on rapid evolutionary timescales. Annu. Rev. Genet. *55*, 401–425. https://doi.org/10.1146/annurev-genet-071719-020301.
21. Thakur, J., Packiaraj, J., and Henikoff, S. (2021). Sequence, chromatin and evolution of satellite DNA. Int. J. Mol. Sci. *22*, 4309. https://doi.org/10.3390/ijms22094309.

22. McLaughlin, R.N., Jr., and Malik, H.S. (2017). Genetic conflicts: the usual suspects and beyond. J. Exp. Biol. *220*, 6–17. https://doi.org/10.1242/jeb.148148.

23. Rosin, L.F., and Mellone, B.G. (2017). Centromeres drive a hard bargain. Trends Genet. *33*, 101–117. https://doi.org/10.1016/j.tig.2016.12.001.

24. Fishman, L., and Willis, J.H. (2005). A novel meiotic drive locus almost completely distorts segregation in mimulus (monkeyflower) hybrids. Genetics *169*, 347–353. https://doi.org/10.1534/genetics.104.032789.

25. Fishman, L., and Saunders, A. (2008). Centromere-associated female meiotic drive entails male fitness costs in monkeyflowers. Science *322*, 1559–1562. https://doi.org/10.1126/science.1161406.

26. Iwata-Otsubo, A., Dawicki-McKenna, J.M., Akera, T., Falk, S.J., Chmátal, L., Yang, K., Sullivan, B.A., Schultz, R.M., Lampson, M.A., and Black, B.E. (2017). Expanded satellite repeats amplify a discrete CENP-A nucleosome assembly site on chromosomes that drive in female meiosis. Curr. Biol. *27*, 2365–2373.e8. https://doi.org/10.1016/j.cub.2017.06.069.

27. Akera, T., Trimm, E., and Lampson, M.A. (2019). Molecular strategies of meiotic cheating by selfish centromeres. Cell *178*, 1132–1144.e10. https://doi.org/10.1016/j.cell.2019.07.001.

28. Fishman, L., and Kelly, J.K. (2015). Centromere-associated meiotic drive and female fitness variation in Mimulus. Evolution *69*, 1208–1218. https://doi.org/10.1111/evo.12661.

29. Wu, T., Lane, S.I.R., Morgan, S.L., and Jones, K.T. (2018). Spindle tubulin and MTOC asymmetries may explain meiotic drive in oocytes. Nat. Commun. *9*, 2952. https://doi.org/10.1038/s41467-018-05338-7.

30. Akera, T., Chmátal, L., Trimm, E., Yang, K., Aonbangkhen, C., Chenoweth, D.M., Janke, C., Schultz, R.M., and Lampson, M.A. (2017). Spindle asymmetry drives non-Mendelian chromosome segregation. Science *358*, 668–672. https://doi.org/10.1126/science.aan0092.

31. Talbert, P.B., Masuelli, R., Tyagi, A.P., Comai, L., and Henikoff, S. (2002). Centromeric localization and adaptive evolution of an Arabidopsis histone H3 variant. Plant Cell *14*, 1053–1066. https://doi.org/10.1105/tpc.010425.

32. Yuan, J., Guo, X., Hu, J., Lv, Z., and Han, F. (2015). Characterization of two CENH3 genes and their roles in wheat evolution. New Phytol. *206*, 839–851. https://doi.org/10.1111/nph.13235.

33. Pontremoli, C., Forni, D., Pozzoli, U., Clerici, M., Cagliani, R., and Sironi, M. (2021). Kinetochore proteins and microtubule-destabilizing factors are fast evolving in eutherian mammals. Mol. Ecol. *30*, 1505–1515. https://doi.org/10.1111/mec.15812.

34. Chmátal, L., Gabriel, S.I., Mitsainas, G.P., Martínez-Vargas, J., Ventura, J., Searle, J.B., Schultz, R.M., and Lampson, M.A. (2014). Centromere strength provides the cell biological basis for meiotic drive and karyotype evolution in mice. Curr. Biol. *24*, 2295–2300. https://doi.org/10.1016/j.cub.2014.08.017.

35. Gascoigne, K.E., Takeuchi, K., Suzuki, A., Hori, T., Fukagawa, T., and Cheeseman, I.M. (2011). Induced ectopic kinetochore assembly bypasses the requirement for CENP-A nucleosomes. Cell *145*, 410–422. https://doi.org/10.1016/j.cell.2011.03.031.

36. Schleiffer, A., Maier, M., Litos, G., Lampert, F., Hornung, P., Mechtler, K., and Westermann, S. (2012). CENP-T proteins are conserved centromere receptors of the Ndc80 complex. Nat. Cell Biol. *14*, 604–613. https://doi.org/10.1038/ncb2493.

37. Malvezzi, F., Litos, G., Schleiffer, A., Heuck, A., Mechtler, K., Clausen, T., and Westermann, S. (2013). A structural basis for kinetochore recruitment of the Ndc80 complex via two distinct centromere receptors. EMBO J. *32*, 409–423. https://doi.org/10.1038/emboj.2012.356.

38. Nishino, T., Rago, F., Hori, T., Tomii, K., Cheeseman, I.M., and Fukagawa, T. (2013). CENP-T provides a structural platform for outer kinetochore assembly. EMBO J. *32*, 424–436. https://doi.org/10.1038/emboj.2012.348.

39. Rago, F., Gascoigne, K.E., and Cheeseman, I.M. (2015). Distinct organization and regulation of the outer kinetochore KMN network downstream of CENP-C and CENP-T. Curr. Biol. *25*, 671–677. https://doi.org/10.1016/j.cub.2015.01.059.

40. Nishino, T., Takeuchi, K., Gascoigne, K.E., Suzuki, A., Hori, T., Oyama, T., Morikawa, K., Cheeseman, I.M., and Fukagawa, T. (2012). CENP-T-W-S-X forms a unique centromeric chromatin structure with a histone-like fold. Cell *148*, 487–501. https://doi.org/10.1016/j.cell.2011.11.061.

41. Hori, T., Amano, M., Suzuki, A., Backer, C.B., Welburn, J.P., Dong, Y., McEwen, B.F., Shang, W.H., Suzuki, E., Okawa, K., et al. (2008). CCAN makes multiple contacts with centromeric DNA to provide distinct pathways to the outer kinetochore. Cell *135*, 1039–1052. https://doi.org/10.1016/j.cell.2008.10.019.

42. Yatskevich, S., Muir, K.W., Bellini, D., Zhang, Z., Yang, J., Tischer, T., Predin, M., Dendooven, T., McLaughlin, S.H., and Barford, D. (2022). Structure of the human inner kinetochore bound to a centromeric CENP-A nucleosome. Science *376*, 844–852. https://doi.org/10.1126/science.abn3810.

43. Das, A., Iwata-Otsubo, A., Destouni, A., Dawicki-McKenna, J.M., Boese, K.G., Black, B.E., and Lampson, M.A. (2022). Epigenetic, genetic and maternal effects enable stable centromere inheritance. Nat. Cell Biol. *24*, 748–756. https://doi.org/10.1038/s41556-022-00897-w.

44. Dittmar, E.L., Oakley, C.G., Conner, J.K., Gould, B.A., and Schemske, D.W. (2016). Factors influencing the effect size distribution of adaptive substitutions. Proc. Biol. Sci. *283*, 20153065. https://doi.org/10.1098/rspb.2015.3065.

45. Rosin, L., and Mellone, B.G. (2016). Co-evolving CENP-A and CAL1 domains mediate centromeric CENP-A deposition across Drosophila species. Dev. Cell *37*, 136–147. https://doi.org/10.1016/j.devcel.2016.03.021.

46. Takeuchi, H., Nagahara, S., Higashiyama, T., and Berger, F. (2024). The chaperone NASP contributes to de novo deposition of the centromeric histone variant CENH3 in Arabidopsis Early embryogenesis. Plant Cell Physiol. *65*, 1135–1148. https://doi.org/10.1093/pcp/pcae030.

47. Pesenti, M.E., Raisch, T., Conti, D., Walstein, K., Hoffmann, I., Vogt, D., Prumbaum, D., Vetter, I.R., Raunser, S., and Musacchio, A. (2022). Structure of the human inner kinetochore CCAN complex and its significance for human centromere organization. Mol. Cell *82*, 2113–2131.e8. https://doi.org/10.1016/j.molcel.2022.04.027.

48. Lin, Z., Akin, H., Rao, R., Hie, B., Zhu, Z., Lu, W., Smetanin, N., Verkuil, R., Kabeli, O., Shmueli, Y., et al. (2023). Evolutionary-scale prediction of atomic-level protein structure with a language model. Science *379*, 1123–1130. https://doi.org/10.1126/science.ade2574.

49. Weissenow, K., Heinzinger, M., Steinegger, M., and Rost, B. (2022). Ultra-fast protein structure prediction to capture effects of sequence variation in mutation movies. Preprint at bioRxiv. https://doi.org/10.1101/2022.11.14.516473.

50. Kandathil, S.M., Lau, A.M., and Jones, D.T. (2023). Machine learning methods for predicting protein structure from single sequences. Curr. Opin. Struct. Biol. *81*, 102627. https://doi.org/10.1016/j.sbi.2023.102627.

51. Guenatri, M., Bailly, D., Maison, C., and Almouzni, G. (2004). Mouse centric and pericentric satellite repeats form distinct functional heterochromatin. J. Cell Biol. *166*, 493–505. https://doi.org/10.1083/jcb.200403109.

52. Dudka, D., Dawicki-McKenna, J.M., Sun, X., Beeravolu, K., Akera, T., Lampson, M.A., and Black, B.E. (2025). Satellite DNA shapes dictate pericentromere packaging in female meiosis. Nature. https://doi.org/10.1038/s41586-024-08374-0.

53. Foltz, D.R., Jansen, L.E.T., Black, B.E., Bailey, A.O., Yates, J.R., 3rd, and Cleveland, D.W. (2006). The human CENP-A centromeric nucleosome-associated complex. Nat. Cell Biol. *8*, 458–469. https://doi.org/10.1038/ncb1397.

54. Arora, U.P., Sullivan, B.A., and Dumont, B.L. (2023). Variation in the CENP-A sequence association landscape across diverse inbred mouse strains. Cell Rep. *42*, 113178. https://doi.org/10.1016/j.celrep.2023.113178.

55. Melters, D.P., Bradnam, K.R., Young, H.A., Telis, N., May, M.R., Ruby, J.G., Sebra, R., Peluso, P., Eid, J., Rank, D., et al. (2013). Comparative analysis of tandem repeats from hundreds of species reveals unique

insights into centromere evolution. Genome Biol. *14*, R10. https://doi.org/10.1186/gb-2013-14-1-r10.

56. Finseth, F.R., Nelson, T.C., and Fishman, L. (2021). Selfish chromosomal drive shapes recent centromeric histone evolution in monkeyflowers. PLoS Genet. *17*, e1009418. https://doi.org/10.1371/journal.pgen.1009418.
57. Birchler, J.A., and Presting, G.G. (2012). Retrotransposon insertion targeting: a mechanism for homogenization of centromere sequences on nonhomologous chromosomes. Genes Dev. *26*, 638–640. https://doi.org/10.1101/gad.191049.112.
58. Waye, J.S., and Willard, H.F. (1989). Concerted evolution of alpha satellite DNA: evidence for species specificity and a general lack of sequence conservation among alphoid sequences of higher primates. Chromosoma *98*, 273–279. https://doi.org/10.1007/BF00327313.
59. Logsdon, G.A., Rozanski, A.N., Ryabov, F., Potapova, T., Shepelev, V.A., Catacchio, C.R., Porubsky, D., Mao, Y., Yoo, D., Rautiainen, M., et al. (2024). The variation and evolution of complete human centromeres. Nature *629*, 136–145. https://doi.org/10.1038/s41586-024-07278-3.
60. Rudd, M.K., Wray, G.A., and Willard, H.F. (2006). The evolutionary dynamics of alpha-satellite. Genome Res. *16*, 88–96. https://doi.org/10.1101/gr.3810906.
61. Cazaux, B., Catalan, J., Justy, F., Escudé, C., Desmarais, E., and Britton-Davidian, J. (2013). Evolution of the structure and composition of house mouse satellite DNA sequences in the subgenus Mus (Rodentia: Muridea): a cytogenomic approach. Chromosoma *122*, 209–220. https://doi.org/10.1007/s00412-013-0402-4.
62. Drpic, D., Almeida, A.C., Aguiar, P., Renda, F., Damas, J., Lewin, H.A., Larkin, D.M., Khodjakov, A., and Maiato, H. (2018). Chromosome segregation is biased by kinetochore size. Curr. Biol. *28*, 1344–1356.e5. https://doi.org/10.1016/j.cub.2018.03.023.
63. Finseth, F.R., Dong, Y., Saunders, A., and Fishman, L. (2015). Duplication and adaptive evolution of a key centromeric protein in mimulus, a genus with female meiotic drive. Mol. Biol. Evol. *32*, 2694–2706. https://doi.org/10.1093/molbev/msv145.
64. Zedek, F., and Bureš, P. (2016). CenH3 evolution reflects meiotic symmetry as predicted by the centromere drive model. Sci. Rep. *6*, 33308. https://doi.org/10.1038/srep33308.
65. Dattoli, A.A., Carty, B.L., Kochendoerfer, A.M., Morgan, C., Walshe, A.E., and Dunleavy, E.M. (2020). Asymmetric assembly of centromeres epigenetically regulates stem cell fate. J. Cell Biol. *219*, e201910084. https://doi.org/10.1083/jcb.201910084.
66. Carty, B.L., Dattoli, A.A., and Dunleavy, E.M. (2021). CENP-C functions in centromere assembly, the maintenance of CENP-A asymmetry and epigenetic age in Drosophila germline stem cells. PLoS Genet. *17*, e1009247. https://doi.org/10.1371/journal.pgen.1009247.
67. Kochendoerfer, A.M., Keegan, R.S., and Dunleavy, E.M. (2023). Centromere proteins are asymmetrically distributed between newly divided germline stem and daughter cells and maintain a balanced niche in Drosophila males. Mol. Biol. Cell *34*, ar42. https://doi.org/10.1091/mbc.E22-10-0466.
68. Ranjan, R., Snedeker, J., and Chen, X. (2019). Asymmetric centromeres differentially coordinate with mitotic machinery to ensure biased sister chromatid segregation in germline stem cells. Cell Stem Cell *25*, 666–681.e5. https://doi.org/10.1016/j.stem.2019.08.014.
69. Lu, K., Jensen, L., Lei, L., and Yamashita, Y.M. (2017). Stay connected: A germ cell strategy. Trends Genet. *33*, 971–978. https://doi.org/10.1016/j.tig.2017.09.001.
70. Spradling, A.C., Niu, W., Yin, Q., Pathak, M., and Maurya, B. (2022). Conservation of oocyte development in germline cysts from Drosophila to mouse. eLife *11*, e83230. https://doi.org/10.7554/eLife.83230.
71. Niu, W., and Spradling, A.C. (2022). Mouse oocytes develop in cysts with the help of nurse cells. Cell *185*, 2576–2590.e12. https://doi.org/10.1016/j.cell.2022.05.001.
72. Basilico, F., Maffini, S., Weir, J.R., Prumbaum, D., Rojas, A.M., Zimniak, T., De Antoni, A., Jeganathan, S., Voss, B., van Gerwen, S., et al. (2014). The pseudo GTPase CENP-M drives human kinetochore assembly. eLife *3*, e02978. https://doi.org/10.7554/eLife.02978.
73. McKinley, K.L., Sekulic, N., Guo, L.Y., Tsinman, T., Black, B.E., and Cheeseman, I.M. (2015). The CENP-L-N complex forms a critical node in an integrated meshwork of interactions at the centromere-kinetochore interface. Mol. Cell *60*, 886–898. https://doi.org/10.1016/j.molcel.2015.10.027.
74. Kasinathan, S., and Henikoff, S. (2018). Non-B-form DNA is enriched at centromeres. Mol. Biol. Evol. *35*, 949–962. https://doi.org/10.1093/molbev/msy010.
75. Scelfo, A., and Fachinetti, D. (2019). Keeping the centromere under control: A promising role for DNA methylation. Cells *8*, 912. https://doi.org/10.3390/cells8080912.
76. García Del Arco, A., and Erhardt, S. (2017). Post-translational modifications of centromeric chromatin. Prog. Mol. Subcell. Biol. *56*, 213–231. https://doi.org/10.1007/978-3-319-58592-5_9.
77. Senaratne, A.P., Muller, H., Fryer, K.A., Kawamoto, M., Katsuma, S., and Drinnenberg, I.A. (2021). Formation of the CenH3-deficient holocentromere in Lepidoptera avoids active chromatin. Curr. Biol. *31*, 173–181.e7. https://doi.org/10.1016/j.cub.2020.09.078.
78. Ding, Y., Kaido, M., Llano, E., Pendas, A.M., and Kitajima, T.S. (2018). The post-anaphase SUMO pathway ensures the maintenance of centromeric cohesion through meiosis I-II transition in mammalian oocytes. Curr. Biol. *28*, 1661–1669.e4. https://doi.org/10.1016/j.cub.2018.04.019.
79. Miyanari, Y., Ziegler-Birling, C., and Torres-Padilla, M.E. (2013). Live visualization of chromatin dynamics with fluorescent TALEs. Nat. Struct. Mol. Biol. *20*, 1321–1324. https://doi.org/10.1038/nsmb.2680.
80. Stirling, D.R., Swain-Bowden, M.J., Lucas, A.M., Carpenter, A.E., Cimini, B.A., and Goodman, A. (2021). CellProfiler 4: improvements in speed, utility and usability. BMC Bioinformatics *22*, 433. https://doi.org/10.1186/s12859-021-04344-9.
81. Schindelin, J., Arganda-Carreras, I., Frise, E., Kaynig, V., Longair, M., Pietzsch, T., Preibisch, S., Rueden, C., Saalfeld, S., Schmid, B., et al. (2012). Fiji: an open-source platform for biological-image analysis. Nat. Methods *9*, 676–682. https://doi.org/10.1038/nmeth.2019.
82. Morgenstern, J.P., and Land, H. (1990). Advanced mammalian gene transfer: high titre retroviral vectors with multiple drug selection markers and a complementary helper-free packaging cell line. Nucleic Acids Res. *18*, 3587–3596. https://doi.org/10.1093/nar/18.12.3587.
83. Swartz, S.Z., McKay, L.S., Su, K.C., Bury, L., Padeganeh, A., Maddox, P.S., Knouse, K.A., and Cheeseman, I.M. (2019). Quiescent cells actively replenish CENP-A nucleosomes to maintain centromere identity and proliferative potential. Dev. Cell *51*, 35–48.e7. https://doi.org/10.1016/j.devcel.2019.07.016.
84. Clift, D., McEwan, W.A., Labzin, L.I., Konieczny, V., Mogessie, B., James, L.C., and Schuh, M. (2017). A method for the acute and rapid degradation of endogenous proteins. Cell *171*, 1692–1706.e18. https://doi.org/10.1016/j.cell.2017.10.033.

Please cite this article in press as: Dudka et al., Adaptive evolution of CENP-T modulates centromere binding, Current Biology (2025), https://doi.org/10.1016/j.cub.2025.01.017

STAR★METHODS

KEY RESOURCES TABLE

REAGENT or RESOURCE	SOURCE	IDENTIFIER
Antibodies		
Rabbit polyclonal anti-mouse N-term CENP-T	This paper	N/A
Mouse monoclonal anti-human HEC1	Santa Cruz	sc-515550, clone C-11
Rabbit monoclonal anti-HMGA1	abcam	ab226112, Clone EPR7839
GFP Booster Alexa Fluor488	ChromoTek	gb2AF488; RRID:AB_2827573
Human polyclonal Anti-Centromere Antibody	Antibodies Incorporated	15-234; RRID:AB_2687472
Cy3 AffiniPure Donkey anti-human IgG (H+L)	Jackson ImmunoResearch Laboratories	AB_2340535; RRID:AB_2340535
Donkey anti-rabbit IgG (H+L) AlexaFluor488	Invitrogen	A21206; RRID:AB_2535792
Goat anti-mouse IgG (H+L) AlexaFluor594	Invitrogen	A11032; RRID:AB_2534091
Bacterial and virus strains		
Stellar Competent Cells	Takara	636763
Chemicals, peptides, and recombinant proteins		
CARD HyperOva	Cosmo Bio	KYD-010-EX-X5
Pregnant Mare Serum Gonadotropin (PMSG)	vivitide	HOR-272
Milrinone	Sigma	M4659
Mineral Oil	Fuji Film Irvine	9305-500 ml
IGEPAL CA-630	Sigma	I8896
TRIzol	Invitrogen	15596026
SuperScript III First Synthesis kit	Invitrogen	18080051
KAPA HiFi HotStart ReadyMix	Roche	KK2602
NucleoSpin Gel and PCR Clean-Up	Takara	740609
In-Fusion Snap Assembly Master Mix	Takara	638948
QuikChange Multi Site-Directed Mutagenesis kit	Agilent	200515
NucleoSpin Plasmid	Takara	740588
T7 mScript Standard mRNA Production System Cell Script	CELLSCRIPT	C-MSC100625
MEGAclear Transcription Clean-Up Kit	Thermo Fisher Scientific	AM1908
GeneArt Precision gRNA Synthesis Kit	Thermo Fisher Scientific	A29377
Vectashield with DAPI	Vector Laboratories	H-1200
Hoechst-33342	Invitrogen	H3570
Q5 High-Fidelity 2X Master Mix	New England Biolabs	M0492
QIAquick PCR Purification Kit	Qiagen	28104
XHO1	New England Biolabs	R0146
ECOR1	New England Biolabs	R0101
T4 DNA polymerase	New England Biolabs	M0203
Mach1 Competent Cells	ThermoFisher Scientific	C862003
QIAprep Spin Miniprep kit	Qiagen	27104
Effectene Transfection Reagent	Qiagen	301425
Experimental models: Cell lines		
HeLa	Cheeseman Lab	N/A
NIH-3T3	ATCC	CRL-1658
Rat2	ATCC	CRL-1764
HEK293GP	Cheeseman Lab	N/A
cALN231 NIH-3T3 + pALN130	This paper	N/A
cALN233 NIH-3T3 + pALN132	This paper	N/A
cALN258 NIH-3T3 + pALN148	This paper	N/A

(*Continued on next page*)

Please cite this article in press as: Dudka et al., Adaptive evolution of CENP-T modulates centromere binding, Current Biology (2025), https://doi.org/10.1016/j.cub.2025.01.017

Continued

REAGENT or RESOURCE	SOURCE	IDENTIFIER
cALN268 Rat2 + pALN130	This paper	N/A
cALN269 Rat2 + pALN132	This paper	N/A
cALN270 Rat2 + pALN148	This paper	N/A
cALN265 HeLa + pALN130	This paper	N/A
cALN266 HeLa + pALN132	This paper	N/A
cALN267 HeLa + pALN148	This paper	N/A
Experimental models: Organisms/strains		
CF-1 mice	Envigo	NSA, stock 033
C57BL/6J mice	Jackson Laboratory	000664
Transgenic *Cenpt*^{RnHFD} mice (in C57BL/6NTac background)	This paper	N/A
Oligonucleotides		
See Table S1 for all primers used	N/A	N/A
Recombinant DNA		
pGEMHE-Sgo2-24xGCN	Ding et al.[78]	Gift from T. Kitajima
pGEMHE-MmCENPT-GFP	This paper	N/A
pGEMHE-MmCENPT-MsHFD-GFP	This paper	N/A
pGEMHE-MmCENPT-McHFD-GFP	This paper	N/A
pGEMHE-MmCENPT-RpHFD-GFP	This paper	N/A
pGEMHE-MmCENPT-RnHFD-GFP	This paper	N/A
pGEMHE-MmCENPT-ASD2HFD-GFP	This paper	N/A
pGEMHE-MmCENPT-4NS-GFP	This paper	N/A
pGEMHE-MmCENPT-RnHFD-4NS-GFP	This paper	N/A
pGEMHE-MmCENP-W	This paper	N/A
pTALYM3B15	Miyanari et al.[79]	Addgene plasmid #47878
pIVT-dCas9-mCherry	Kumon et al.[16]	Addgene plasmid #174443
pGEMHE-Trim21-OLLAS	Dudka et al.[52]	N/A
pALN130 GFP-MmCENPT	This paper	N/A
pALN132 GFP-MmCENP-T-RnHFD	This paper	N/A
pALN148 GFP-MmCENPT-RnHFD-4NS	This paper	N/A
Software and algorithms		
FREEDA	Dudka et al.[17]	https://github.com/DDudka9/freeda/releases or https://www.tamarind.bio/freeda
Centrocalc	Dudka et al.[17]	https://github.com/DDudka9/Centrocalc
Cell Profiler	Stirling et al.[80]	https://cellprofiler.org/
ImageJ (Fiji)	Schindelin et al.[81]	https://fiji.sc/
GraphPad Prism v10	GraphPad	https://www.graphpad.com/
Other		
Amicon Ultra-0.5 100-K columns	Sigma	UFC5100625

EXPERIMENTAL MODEL AND STUDY PARTICIPANT DETAILS

Mice

Commercially available CF1 strain was purchased from Envigo (NSA, stock# 033). Chimeric mice with chimeric CENP-T allele (Cenpt^{RnHFD}) were custom generated by The Taconic-Cyagen Model Generation Alliance (Taconic Biosciences GmbH, Germany) in the C57BL/6NTac background using CRISPR/Cas9 knock-in strategy. Briefly, the mouse Cenpt gene locus from partial exon 11 to partial exon 13 encoding the 413-503aa region of mouse CENP-T protein (ensembl transcript ID: ENSMUST00000040776) was swapped with the corresponding region of the rat CENP-T coding sequence (ensembl transcript ID: ENSRNOT00000036702.5) using two pairs of guide RNAs, Cas9 enzyme and repair template microinjected into a fertilized egg. Tissue Preparation Solution (Sigma; T3073), Extraction Solution (Sigma; T7526), Neutralization Solution (N3910) and REDExtract N-AMP PCR ReadyMix (Sigma;

Please cite this article in press as: Dudka et al., Adaptive evolution of CENP-T modulates centromere binding, Current Biology (2025), https://doi.org/10.1016/j.cub.2025.01.017

R4775) were used for DNA extraction and amplification. Forward primer annealing to both alleles (between exon 10 and 11 of mouse Cenpt) and two allele-specific reverse primers (exon 11 of rat Cenpt or between exons 11 and 12 of mouse Cenpt) were used for genotyping. See Table S1 for primer sequences. Heterozygous founder mice ($Cenpt^{MmHFD/RnHFD}$) were crossed to one another or to WT C57BL/6J strain (Jackson Laboratory, 000664) to minimize impact of off-target mutations, and heterozygous pups of those matings were crossed together to generate isogenic heterozygous animals (see Figure S2B). To confirm equal expression, 49 CENP-T transcripts were independently sampled from testis of two heterozygous males and scored for presence of either mouse or rat HFD. Briefly, testes were independently dissected and homogenized (KIMBLE Dounce glass tissue grinder; Sigma D9938), total RNA was isolated (TRIzol; Invitrogen; 15596026), and cDNA was prepared (SuperScript III First Synthesis kit; Invitrogen; 18080051). The entire CENP-T coding sequence was amplified by PCR (KAPA HiFi HotStart ReadyMix; Roche; KK2602), isolated from a polyacrylamide gel (NucleoSpin Gel and PCR Clean-Up; Takara; 740609), cloned (In-Fusion Snap Assembly Master Mix; Takara; 638948) into pGEMHE plasmids (kind gift from T. Kitajima), amplified in E. coli (Stellar Competent Cells; Takara; 636763), isolated (NucleoSpin Plasmid; Takara; 740588), and each clone was sequenced (Azenta Life Sciences) (see Figures S2A and S2C). Heterozygous pups were then crossed to one another to derive isogenic homozygous WT ($Cenpt^{MmHFD/MmHFD}$) or chimeric ($Cenpt^{RnHFD/RnHFD}$) lines (see Figure S2B). Mice were housed in controlled room temperature conditions with minimal disturbances, light/dark cycle of 12 h each, and humidity ranging between 30-70% depending on the season. All animals used for oocyte and sperm collection and immunofluorescence experiments were re-genotyped when sacrificed. All experiments were performed in 6-11 weeks old animals using age-matched controls sacrificed on the same day. All animal experiments and protocols were approved by the Institutional Animal Use and Care Committee of the University of Pennsylvania and were consistent with National Institutes of Health guidelines (protocol #804882).

Cell lines

All cell lines were cultured in DMEM supplemented with 10% tetracycline-free fetal bovine serum (FBS), 100 units/ml penicillin, 100 units/ml streptomycin, and 2 mM l-glutamine at 37°C with 5% CO_2. Cell lines were tested monthly for mycoplasma contamination and validated based on the presence of appropriate cellular behaviors and markers. Polyclonal cell lines stably expressing N-terminal mEGFP fusions for CENPT were generated using retroviral infection in NIH-3T3, Rat2, and HeLa cells. GFP positive cells were enriched by fluorescence automated cell sorting 2 days after transduction and cultured as described above.

METHOD DETAILS

Plasmid generation

All CENP-T and CENP-W coding sequences were cloned by PCR (KAPA HiFi HotStart ReadyMix; Roche; KK2602) using cDNA obtained from tissue samples of selected species as template. CENP-T coding sequence and tissue sample from *Rhabdomys pumilio* were kindly provided by Ricardo Mallarino (Princeton University). Ancestral HFD was synthesized commercially (Azenta Life Sciences). Mouse CENP-T used in oocyte experiments was cloned into pGEMHE plasmid containing C-terminal GFP separated by 5xGly linker (pGEMHE-CENP-T-GFP). Briefly, CENP-T coding sequence was amplified by PCR (KAPA HiFi HotStart ReadyMix; Roche; KK2602), isolated from a polyacrylamide gel (NucleoSpin Gel and PCR Clean-Up; Takara; 740609), cloned (In-Fusion Snap Assembly Master Mix; Takara; 638948) into pGEMHE plasmids (kind gift from T. Kitajima; [78]), amplified in E. coli (Stellar Competent Cells; Takara; 636763), isolated (NucleoSpin Plasmid; Takara; 740588), and each clone was sequenced (Azenta Life Sciences). Chimeric CENP-T variants were generated by subcloning divergent HFDs into the pGEMHE-CENP-T-GFP plasmid. Note that the last 12 amino acids (histone fold extension) remained unchanged. 4NS mutants were generated using site-directed mutagenesis (QuikChange Multi Site-Directed Mutagenesis Kit; Agilent; 200515). Mouse CENP-W was cloned untagged into a pGEMHE plasmid backbone (pGEMHE-CENP-W). The identity of all constructs was confirmed using Sanger sequencing of the entire coding sequence. pIVT-dCas9-mCherry expressing catalytically dead Cas9 targeting minor satellite via a guide RNA recognizing "5′-ACACTGAAAAA CACATTCGT-3′" sequence was generated previously[16]; pTALYM3-TALE-mClover expressing a TALE protein recognizing "5′-TGCCATATTCCACGT-3" sequence of the major satellite repeat[79] was a kind gift from Maria-Elena Torres-Padilla (Addgene; #47874). Minor satellite guide RNA was synthesized using GeneArt Precision gRNA Synthesis Kit (Thermo Fisher Scientific; A29377). For expression of fusion proteins in somatic cell lines, CENPT coding sequences were amplified from pGEMHE plasmids and cloned into pBABE derived retroviral expression vectors containing N.Terminal enhanced GFP (EGFP) with a monomerizing A206K mutation and a Tev-S linker (pALNXXX-EGFP-CENPT). In brief, CENPT coding sequences were amplified by PCR (Q5 High-Fidelity 2X Master Mix; New England Biolabs; M0492), isolated from a polyacrylamide gel (QIAquick PCR Purification Kit; Qiagen; 28104), digested via XHO1 (New England Biolabs; R0146) and ECOR1 (New England Biolabs; R0101) and ligated into pBABE derived plasmids (T4 DNA polymerase; New England Biolabs; M0203). Plasmids were then amplified in E. coli (Mach1 Competent Cells; ThermoFisher Sci.; C862003), isolated (QIAprep Spin Miniprep kit; Qiagen; 27104), and each clone was sequenced (Azenta Life Sciences). The identity of all constructs was confirmed using Sanger sequencing of the entire coding sequence. See Table S1 for primer sequences.

Retrovirus preparation and transduction

For retroviral production, HEK-293GP cells were seeded at a density of 4 million cells in 10 mL complete media in 10 cm plates. After 24 hours, cells were transfected with a mix containing 2.5 mg VSVG packaging plasmid and 5 mg pBABE-based vectors containing

Please cite this article in press as: Dudka et al., Adaptive evolution of CENP-T modulates centromere binding, Current Biology (2025), https://doi.org/10.1016/j.cub.2025.01.017

EGFP-CENPT fusions in 300 mL Buffer EC with 16 mL Enhancer and 60 mL Effectene (Effectene Transfection Reagent; Qiagen; 301425) for transduction as described previously.[82] Media was changed 24 hours later to 5 mL fresh complete media. At 48 hours after transfection, virus was collected, filtered through a 0.2 mm filter, and stored at 4° C until use.

Antibody generation

The polyclonal antibody against the mouse CENP-T protein was generated by injection of mouse GST-CENP-T (AA 1-374; pOM17) into rabbits (LabCorp, Inc.). The serum was affinity purified against a truncated version of the mouse CENP-T protein (AA 1-207; pOM18) as described previously[83] including elution with 0.1 M Glycine pH2.6, followed by dialysis into PBS + 50% glycerol.

Oocyte collection and microinjection

Transgenic females expressing chimeric CENP-T or isogenic controls expressing mouse CENP-T were hormonally primed with 150ul of CARD HyperOva (Cosmo Bio; KYD-010-EX-X5). For expression of GFP-tagged CENP-T variants, CF-1 females were primed with 5 U of pregnant mare serum gonadotropin (PMSG; vivitide; HOR-272). 40–48h after priming, germinal vesicle oocytes were collected using M2 media (Sigma; MR-015), denuded from cumulus cells and cultured in Chatot-Ziomek-Bavister media (CZB; Fisher Scientific; MR-019-D) under mineral oil (Fuji Film Irvine; 9305-500 ml) in humidified atmosphere of 5% CO_2 and at 37.8°C. All media were supplemented with 2.5mM of milrinone (Sigma; M4659) to prevent meiotic resumption. Oocytes were incubated for at least 1 h prior to microinjection on a hot plate (38°C) under mineral oil. Oocytes were then microinjected with ~5 pl of mRNAs in M2 medium with 2.5 mM milrinone and 3 mg/ml BSA at RT with a micromanipulator TransferMan NK 2 (Eppendorf) and a picoinjector (Medical Systems Corp). Oocytes were then incubated in 30–50 μl drops of Chatot-Ziomek-Bavister medium (Thermo Fisher Scientific; MR019D) under mineral oil at 37.8°C and 5% CO2 (Airgas) for 16 h to allow protein expression. The concentration of CENP-T mRNA (25–100 ng/μl) was selected to ensure similar cytoplasmic expression of each construct. Mouse CENP-W was used at 100ng/ml concentration. To deplete HMGA1, the Trim-away approach was used.[84] Briefly, milrinone-arrested oocytes were microinjected with ~5 pl mix containing 0.5mg/ml of buffer-exchanged (Amicon Ultra-0.5 100-K columns; Sigma; UFC5100625) recombinant rabbit monoclonal anti-HMGA1 antibodies (EPR7839 clone; ab226112; abcam), supplemented with mRNAs at the following concentrations: TALE-mClover – 200 ng/μl, Trim21-OLLAS – 300-600 ng/μl; dCas9-mCherry – 120-160 ng/μl; gRNA – 20-30ng/μl. mRNAs were synthesized using the T7 mScriptTM Standard mRNA Production System (C-MSC100625; CELLSCRIPT), purified using MEGAclear Transcription Clean-Up Kit (Thermo Fisher Scientific; AM1908) and diluted in water with IGEPAL CA-630 (Sigma; I8896) at 0.05% final concentration to facilitate microinjection. Oocytes were fixed 7h after milrinone washout at metaphase I.

Sperm collection

Sperm was collected from singly housed males by dissection of epididymis (cauda, corpus, caput and vas deferens) in Human Tubal Fluid media (Sigma MR-070-D) supplemented with 3mg/ml Bovine Serum Albumin (BSA; Sigma; A4503) under mineral oil (Fuji Film Irvine; 9305-500 ml) and 15min incubation in humidified atmosphere of 5% CO_2 and at 37.8°C to allow sperm swim-out. Homogenous sperm suspension was obtained by gentle pipetting, and water-immobilized intact sperm cells were counted using a Bright-Line Hemacytometer (Sigma; Z359629).

Image acquisition: oocytes

Metaphase I oocytes were fixed in 2% paraformaldehyde in PBS (pH 7.4) with 0.1-0.5% Triton X-100 for 20 min at RT, permeabilized in PBS with 0.1-0.5% Triton X-100 for 15 min at RT, placed in blocking solution (PBS with 0.3% BSA and 0.01% Tween-20) overnight at 4°C, incubated 1 h with primary antibody in blocking solution, washed three times for 15 min each, incubated 1 h with secondary antibody, washed three times for 15 min each, and mounted in Vectashield with DAPI (H-1200; Vector Laboratories) to visualize chromosomes. Centromeres were labeled with mouse monoclonal anti-human HEC1 antibody (1:100; Santa-Cruz; C-11; sc-515550) or custom-made rabbit polyclonal anti-mouse CENP-T (1:1000; specific to mouse CENP-T N-terminus). Secondary antibodies used: donkey anti-rabbit IgG (H+L) conjugated with AlexaFluor488 (Invitrogen; A21206) and goat anti-mouse IgG (H+L) conjugated with AlexaFluor594 (Invitrogen; A11032). Confocal images were collected as z-stacks of 31 planes at 0.5-μm intervals to visualize the entire metaphase plate, using a confocal microscope (DMI4000B; Leica) equipped with a 63× 1.3 NA glycerol-immersion objective lens, an xy piezo Z stage (Applied Scientific Instrumentation), a spinning disk (Yokogawa Corporation of America), and an electron multiplier charge-coupled device camera (ImageEM C9100-13; Hamamatsu Photonics), controlled by MetaMorph software (Molecular Devices). A Vortran Stradus VersaLase 4 laser module with 405-, 488-, 561-, and 639-nm lasers (Vortran Laser Technology) was used for excitation. Panels of microscopic images were prepared using ImageJ (National Institutes of Health) free software.

Image acquisition: Somatic cells

Cells were seeded onto polylysine-coated coverslips (Sigma-Aldrich) and cultured for 24 hours prior to fixation. Cells were then fixed in 4% formaldehyde in PBS + 0.5% Triton X-100 for 10 mins followed by three consecutive washes in PBS + 0.1% Triton X-100 and blocked in AbDil (20 mM Tris-HCl pH 7.5, 150 mM NaCl, 0.1% Triton X-100, 3% BSA) for 30 min at room temperature. Immunostaining was performed by incubating the coverslips in primary antibody recognizing centromeres (polyclonal human Anti-Centromere protein; 1:200; Antibodies Incorporated; 15-234) diluted in AbDil for 1 hour at room temperature followed by three consecutive washes in PBS + 0.1% Triton X-100. After washing, Cy3-conjugated secondary antibody (Jackson ImmunoResearch Laboratories) was diluted 1:300 in Abdil together with anti-GFP Booster Alexa Fluor 488 (1:200; Chromotek; gb2AF488) and

0.3 mg/mL Hoescht-33342 (1:1000; Invitrogen; H3570), and the sample was incubated for 1 h at room temperature followed by 3 consecutive washes in PBS containing 0.1% Triton X-100. The coverslips were next mounted in p-phenylamine diamine (PPDM) onto slides. Images were acquired on a DeltaVision Core deconvolution microscope (Applied Precision) equipped with a CoolSnap HQ2 CCD camera. Approximately 35 Z-sections were acquired at 0.2 μm steps using a 60×, 1.42 NA Olympus U-PlanApo objective.

Image analysis

Confocal images were analyzed manually (Figures 1D, 1F, 4D, 4E, S1B, and S1D). Briefly, 16-bit images were used, and circular 4-pixel diameter ROIs were drawn to measure centromeric and adjacent cytoplasmic (background) intensities based on sum projections of 5 single meiotic bivalents chosen at random based on the DAPI channel. Intensities of both centromeres in each bivalent were measured (total of 10 centromeres per cell), and background intensity was subtracted. The intensity of each background-subtracted centromere was normalized to the average intensity of all control (mouse CENP-T) background-subtracted centromeres per experiment. Equivalent normalization was done for cytoplasmic intensity measurements. Custom-built Python program Centrocalc[17] available here: https://github.com/DDudka9/Centrocalc was used to quantify data represented in Figures 1E, 2B, 3E, and S1C. Briefly, kinetochores were identified automatically as spots of 150 nm radius, and local maxima were found using CENP-T signal. Up to 38 spots were selected, separated by a minimum two pixels, and 3D ellipsoid regions of 4 × 4 × 3 pixels were drawn. Modifying Centrocalc source code allows parameter customization. Quantifications of fluorescence intensity from mouse, rat and human tissue culture cells represented in Figures 4G–4I were conducted on maximally projected images using FIJI/Image J[81] and Cell Profiler.[80] To quantify the pixel intensity of centromere localized GFP signal, a custom cell profiler pipeline was developed. In brief, individual nuclei were first identified using Hoescht-DNA signal. A secondary mask was then applied in which individual centromeres approximately 5–12 pixel in diameter were identified per nuclei, using enhanced anti-human centromeric antibody signal. Finally, a background intensity measurement was obtained by measuring the pixel intensity 5 pixels outside each identified centromere and subtracted from each centromere intensity measurement. Intensity of each background-subtracted centromere was normalized to average intensity of all control (mouse CENP-T) background-subtracted centromeres per experiment.

Molecular evolution analyses

All analyses were done using a fully automated computational pipeline to detect positive selection, FREEDA,[1,7] available as a desktop application: https://github.com/DDudka9/freeda/releases or accessible via a web server TamarindBio: https://www.tamarind.bio/freeda. Briefly, mouse CENP-T coding sequence (ensembl transcript ID: ENSMUST00000040776) was used as reference to search for Cenpt genes in selected *Murinae* genomes ensuring orthology by synteny analysis, followed by exons retrieval, multiple sequence alignment, gene tree generation and detection of sites that most likely evolved under positive selection using CODEML site models M7 v M8 assuming F3x4 codon frequency and posterior probability >=0.8 (PAML[9]). 12 orthologous CENP-T coding sequences were successfully identified from the following GenBank assemblies: *Mus spretus* (GCA_001624865.1), *Mus caroli* (GCA_900094665.2), *Mus minutoides* (GCA_902729485.2), *Mus pahari* (GCA_900095145.2), *Apodemus speciosus* (GCA_002335545.1), *Praomys delectorum* (GCA_019843815.1), *Mastomys coucha* (GCA_008632895.1), *Grammomys surdaster* (GCA_004785775.1), *Arvicanthis niloticus* (GCA_011762505.1), *Rhynchomys soricoides* (GCA_019843965.1), *Rattus rattus* (GCA_011064425.1), *Rattus norvegicus* (GCA_000001895.4). Ancestral CENP-T HFD was reconstructed in PAML using CENP-T coding sequences from three *Muroidea* genomes as outgroups: *Acomys russatus* (GCA_903995435.1), *Peromyscus maniculatus* (GCA_003704035.3) and *Neotoma lepida* (GCA_001675575.1).

Structure modeling

The ESMFold web server (https://esmatlas.com/resources?action=fold) was used to predict CENP-T HFD structure based on sequences corresponding to mouse CENP- T 413–515aa region. Note that each HFD contains the histone fold extension of mouse CENP-T. Structural similarity was assessed by aligning the predicted models in 3D space (superimposition) using the "align" function in Pymol (The PyMOL Molecular Graphics System, Version 2.0, Schrödinger, LLC) and RMSD (Root-Mean-Square-Deviation) values.

QUANTIFICATION AND STATISTICAL ANALYSIS

Data points are pooled from at least two independent experiments. The following statistical methods were used: unpaired two-tailed t test in Figures 1E, 2D, 2E, and S1C; paired two-tailed t test in Figure S4; Mann-Whitney U two-tailed test in Figures 2B and S2C; ordinary one-way ANOVA with Tukey's multiple comparison test in Figures 1D, 1F, S1B, and S1D; Kruskal-Wallis with Dunn's multiple comparison test in Figures 3E, 4D, 4E, and 4G–4I; chi-square test in Figure 2C. The exact value of n, what n represents, and definition of center can be found in the figure legends for each experiment. All tests were performed using GraphPad Prism; Bayes Empirical Bayes analyses were performed using PAML model 8. Posterior probabilities >= 0.8 were considered significant.